Proposal for a controllable chip-based electrostatic double well for cold-molecule trapping

Qing Liu,[1] Wenli Li,[1] Chenyue Pan,[2] Qi Zhou,[3] Tao Yang,[1,4,5] Shunyong Hou,[1,*] and Jianping Yin[1]
[1]*State Key Laboratory of Precision Spectroscopy, East China Normal University, Shanghai 200062, China*
[2]*China World Academy, Changshu, Jiangsu 215500, China*
[3]*School of Science, East China University of Technology, Jiangxi Nanchang 330013, China*
[4]*Xinjiang Astronomical Observatory, Chinese Academy of Sciences, Urumqi, Xinjiang 830011, China*
[5]*Collaborative Innovation Center of Extreme Optics, Shanxi University, Taiyuan, Shanxi 030006, China*

(Received 12 August 2024; revised 12 October 2024; accepted 27 November 2024; published 19 December 2024)

Over the past two decades, a chip-based atom double well has matured as a powerful art with many applications in modern science. However, its molecular counterpart, which holds potential for higher precision and broader science, has been little studied. In this paper, we propose a scheme for chip-based electrostatic double-well potential for polar molecules. The structure consists of two square wires and three square electrodes deposited on an insulating chip. By adjusting the applied voltages, versatile operations on the double well can be easily realized, such as precisely changing the depth and height of the double well, dynamically deforming the double-well potential to a single well and vice versa, and adjusting the double well from symmetric to asymmetric. We have developed numerical and analytical methods to verify the feasibility of our scheme with both light ($^{15}ND_3$) and heavy ($^{202}Hg^{19}F$) polar molecules. The microscopic integrated double-well potential presents a promising platform for confined molecule interferometry. Also, it provides new perspectives for the study of cold collisions, sympathetic cooling, quantum information processing, and quantum simulation.

DOI: 10.1103/PhysRevA.110.063319

I. INTRODUCTION

Matter-wave interference experiments provide definitive evidence that reveals the wave nature of matter, such as electrons [1,2], neutrons [3], atoms [4], and molecules [5]. Additionally, such experiments offer a unique and subtle probe into the fundamental properties of matter at quantum level [6]. Over the last three decades, atom interferometry has given rise to numerous scientific and technical advancements [7,8] in areas such as frequency metrology and inertial and gravitational field sensing. Moreover, there is an increasing interest in investigating matter-wave interference with more massive and more complex particles, such as molecules [9,10]. This is driven by the potential for higher precision, broader applications, and the exploration of unexplored territories where new physical phenomena might be discovered [11,12]. Examples include the search for the permanent electric dipole moment (eEDM) of electrons [13,14] and the possible time-dependent variation of fundamental constants of nature [15] fifth forces [16,17] and dark matter [18].

In parallel, microscopic integrated matter-wave interference on a chip is attractive for its implementation, since it provides control over quantum systems in compact, robust, and scalable setups [19,20]. Over the past two decades, chip-based atom interferometry has been sophisticatedly developed as an essential tool for both fundamental and applied research areas [21]. In contrast, chip-based molecule interferometry remains in its infancy stage. This situation arises partly because the complexity of the internal structure of molecules makes the preparation and manipulation of ultracold molecular samples challenging. However, recent substantial advancements in the field of cold molecules [22–32], particularly the realization of long-lived degenerate Fermi gases [33–35] and Bose-Einstein condensates [36] of polar molecules, have paved the way for molecule interferometry on a chip. Pioneering works in cooling and manipulating molecules on a chip [37–44] lay the foundation for exploring new frontiers in molecule chips.

Stimulated by the advancements in molecule cooling tools and state-of-the-art microfabrication technology [45], we propose a chip-based electrostatic double well for molecule interferometry. Note that its counterpart, chip-based double well for atom interferometry, has been extensively investigated over the last two decades [46–51]. The double well serves as a fundamental configuration for studying matter-wave dynamics [48], wherein a single trap is initially transformed into a double well, followed by the recombination of the two wells to observe interference. Our scheme comprises two square wires and three square electrodes deposited on an insulating chip, characterized by robustness, scalability, and versatility. It not only allows for the dynamic deformation of the double-well potential into a single well and vice versa, but also facilitates the transition from a symmetric to an asymmetric configuration. We have developed numerical and analytical methods to validate the feasibility of our scheme using both light (ND_3) and heavy ($^{202}Hg^{19}F$) polar molecules. $^{202}Hg^{19}F$ is selected as it is a promising candidate for eEDM measurement and is suitable for laser cooling [52].

II. DESIGN

Figure 1 provides a schematic diagram of the experimental setup for the proposed chip-based electrostatic double

*Contact author: syhou@lps.ecnu.edu.cn

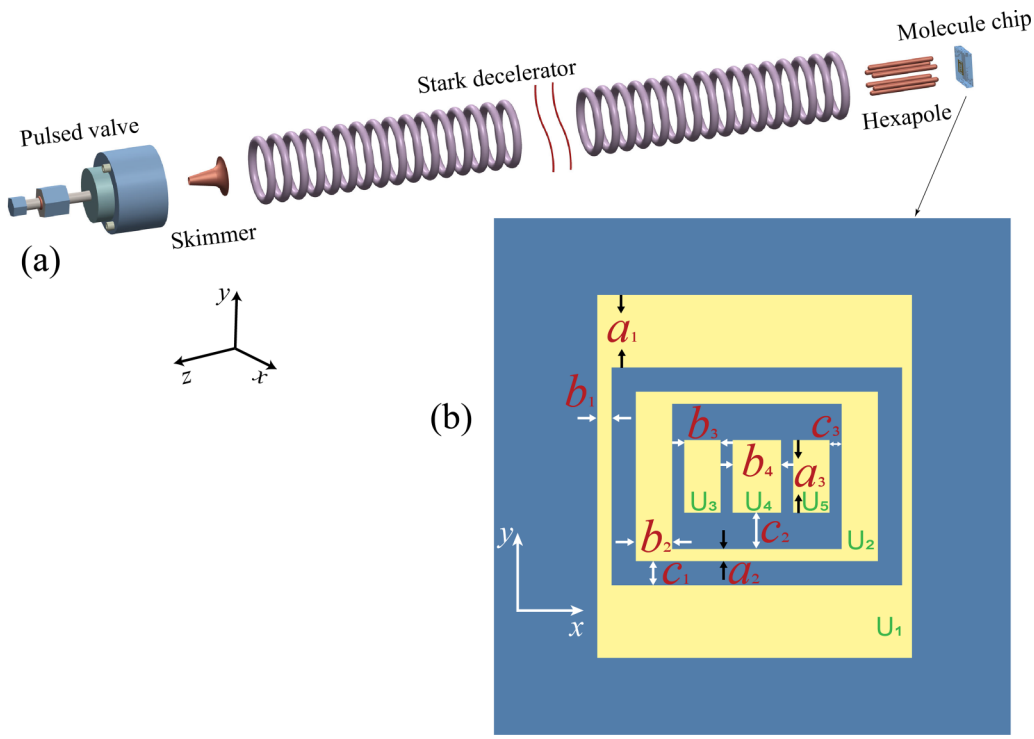

FIG. 1. Proposed experimental setup and chip design. (a) A supersonic beam is generated via a pulsed valve, slowed down by the subsequent Stark decelerator, and then coupled into an electrostatic (double) well on a chip. (b) Expanded view of the electrostatic (double) well structure, together with applied voltage and dimension parameters.

well. Figure 1(a) illustrates a supersonic polar molecular beam being formed via a pulsed valve, passing through a skimmer, and then decelerated by a Stark decelerator. Subsequently, the molecular beam is coupled in the vicinity of the molecule chip. An expanded view of the electrostatic double-well chip is shown in Fig. 1(b), with the substrate being a thin insulating plate. Two square wires and three small rectangular electrodes are deposited on this plate. The outermost square measures $130\,\mu\text{m} \times 150\,\mu\text{m}$ in the x and y directions, respectively. The specific dimensions are as follows: $a_1 = a_3 = 30\,\mu\text{m}$, $a_2 = 5\,\mu\text{m}$, $b_1 = 5\,\mu\text{m}$, $b_2 = b_3 = 15\,\mu\text{m}$, $b_4 = 20\,\mu\text{m}$, $c_1 = 10\,\mu\text{m}$, $c_2 = 15\,\mu\text{m}$, and $c_3 = 5\,\mu\text{m}$. The voltages applied to the different electrodes are labeled as U_1 to U_5. The coordinate system is also depicted in Fig. 1, with the z axis being perpendicular to the molecule chip surface and directed opposite to the molecular beam.

III. THEORETICAL ANALYSIS

Let us derive the electric field distribution on the surface of the chip. In a space devoid of electric charges, the electric potential $\Phi(x, y, z)$ must satisfy Laplace's equation. The expression for the electric potential of our designed chip is given by

$$\Phi(x, y, z) = \sum_{m,n=0}^{\infty} A_{mn} e^{[-z\sqrt{(mk_x)^2+(nk_x)^2}]} \times [\cos(mk_x x)\cos(nk_y y)]. \tag{1}$$

Here, $k_x = 2\pi/L_x$ and $k_y = 2\pi/L_y$. L_x and L_y represent the periodicity (or length) of the potential in the x and y directions, respectively. The coefficients A_{mn} are determined by comparing numerically calculated fields along lines in the x (y) direction, utilizing the same methodology as in Ref. [53]. We select $m = n = 0,\ 1,\ 2,\ 3,\ 4,\ 5$ to generate quadrupole potentials in the transverse directions. As long as the electric potential is constrained, the electric field strength is given by

$$E_i = \frac{\partial \phi}{\partial i}, \tag{2}$$

with $i = x,\ y,\ z$. The magnitude of the electric field near the chip is then derived using the following equation:

$$|\vec{E}| = \sqrt{(E_x)^2 + (E_y)^2 + (E_z)^2}. \tag{3}$$

The interaction between polar molecules and electric fields can be described as follows:

$$\begin{Bmatrix} F_x \\ F_y \\ F_z \end{Bmatrix} = -\left(\frac{1}{|\vec{E}|}\frac{\mathrm{d}W}{\mathrm{d}|\vec{E}|}\right) \begin{Bmatrix} \frac{\partial^2\phi}{\partial x^2} & \frac{\partial^2\phi}{\partial x\partial y} & \frac{\partial^2\phi}{\partial x\partial z} \\ \frac{\partial^2\phi}{\partial x\partial y} & \frac{\partial^2\phi}{\partial y^2} & \frac{\partial^2\phi}{\partial y\partial z} \\ \frac{\partial^2\phi}{\partial x\partial z} & \frac{\partial^2\phi}{\partial y\partial z} & \frac{\partial^2\phi}{\partial z^2} \end{Bmatrix} \begin{Bmatrix} \frac{\partial\phi}{\partial x} \\ \frac{\partial\phi}{\partial y} \\ \frac{\partial\phi}{\partial z} \end{Bmatrix}, \tag{4}$$

where W is the Stark potential. For $^{15}ND_3$ molecules in the $|J, KM\rangle = |1, -1\rangle$ state, the Stark potential $W(|\vec{E}|)$ can be expressed as

$$W(|\vec{E}|) = \sqrt{\left(\frac{W_{\text{inv}}}{2}\right)^2 + \left(\frac{1}{2}\mu|\vec{E}|\right)^2} - \left(\frac{W_{\text{inv}}}{2}\right). \tag{5}$$

Here W_{inv} represents the zero-field inversion splitting and μ denotes the dipole moment. For $^{15}ND_3$, the inversion splitting

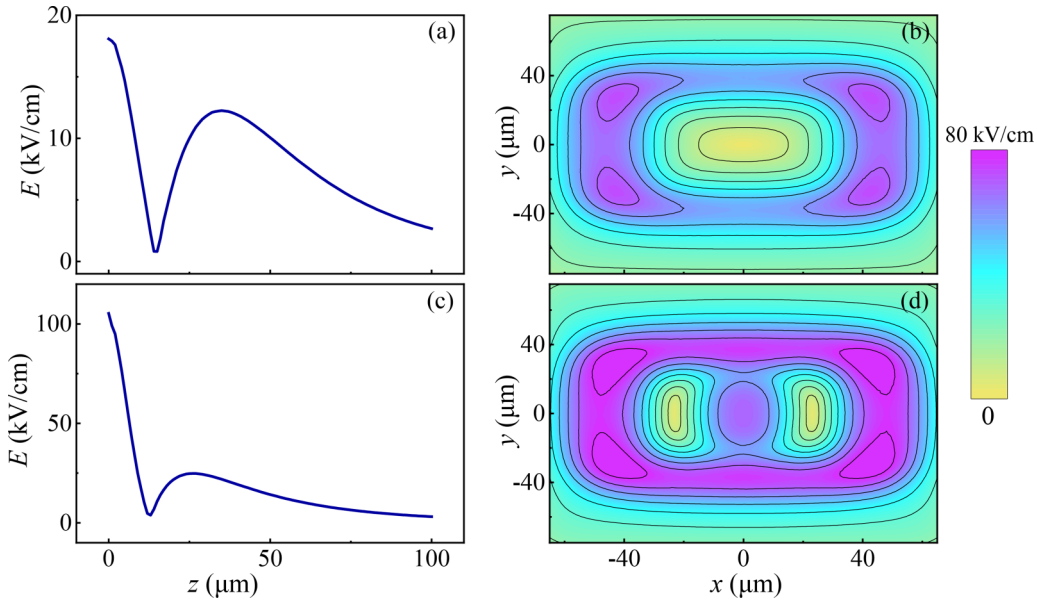

FIG. 2. The distributions of electric field strength along the z axis for the single well (a) and at $x = 23\,\mu$m along the z coordinate for one of the double wells (c). The electric field distributions and the equipotential lines in the x-y plane through the minima of the single well (b) and the double well (d). The minima of both the single and double wells lie on the x axis. Violet indicates higher strength and yellowish green indicates lower strength.

is 1430.3 MHz, and its dipole moment is identical to that of $^{14}ND_3$, i.e., 1.48 D [54].

The electric field distribution on the chip, as derived from Eqs. (1)–(3), is depicted in Fig. 2. In our design, either a single or a double potential well could be formed by applying appropriate voltages on the electrodes. For a single well, the applied voltages are set as follows: $U_1 = 200$ V, $U_2 = -200$ V, *and* $U_3 = U_4 = U_5 = 60$ V. The electric field distributions along the longitudinal direction (z axis) and in the x-y plane through the minimum of the potential well are shown in Figs. 2(a) and 2(b), respectively. The trap depth in the longitudinal direction reaches 0.15 cm^{-1}, enabling the confinement of $^{15}ND_3$ molecules with a maximum velocity of 13.1 m/s. The height of the potential well (i.e., the distance from the minimum of the potential to the surface of the chip) is $\sim$14 μm. When the voltage of U_4 is switched from 60 to -200 V, and the voltages of the other electrodes remain unchanged, a double potential well is formed on the chip surface, as shown in Figs. 2(c) and 2(d). The trap depth in the longitudinal direction reaches 0.30 cm^{-1}, enabling the confinement of $^{15}ND_3$ molecules with a maximum velocity of 18.5 m/s. The height of each potential well is $\sim$13 μm. Figure 3 illustrates how the single potential well deforms into a double well by gradually changing the voltage of U_4 from 60 to -200 V, which causes a barrier to smoothly rise in the center of the single trap, ultimately resulting in a double trap on the chip, and vice versa. At the same time, the distance between the two minima of the double well gradually increases to $\sim$45 μm.

IV. TRAJECTORY CALCULATIONS

In addition to the aforementioned theoretical analysis, the trajectory calculation is employed to quantitatively characterize the microscope compact double-well scheme. For subsequent calculations, two molecular species are chosen as testers: $^{15}ND_3$ in the $|J, KM\rangle = |1, -1\rangle$ state as a typical light molecule, and HgF in the $X^2\Sigma_{1/2}(\upsilon = 0,\ \ N = 2, N_M = 0\ )$ state as a heavy one. The calculations do not take into account molecular losses due to background collisions and nonadiabatic transitions, nor the interaction of molecules with the chip surface due to their significant distances. The trajectory calculations commence with the molecular beam loading onto the chip, proceed through the dynamic processes from a single well to a double well, and end with the adiabatic cooling of molecules within the trap.

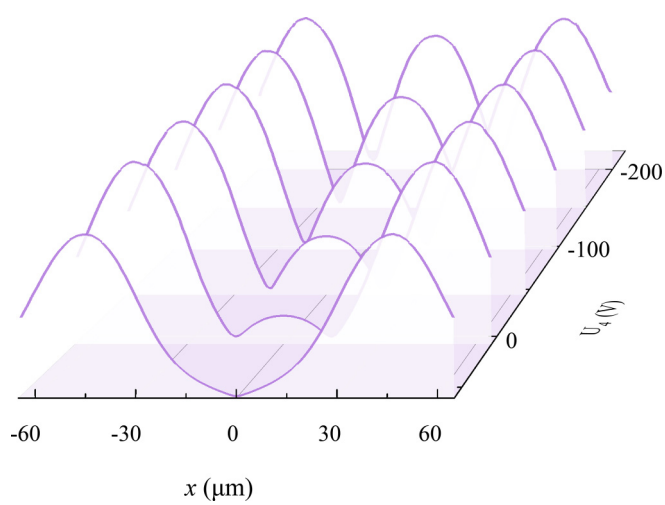

FIG. 3. Smooth deformation from a single trap to a double trap on the chip. The electric field distributions along the x axis through the minimum (minima) of the well(s) as a function of U_4 is presented. As the voltage of U_4 decreases, the barrier in-between the two potentials rises, and the interval between the two minima of the double well increases as well.

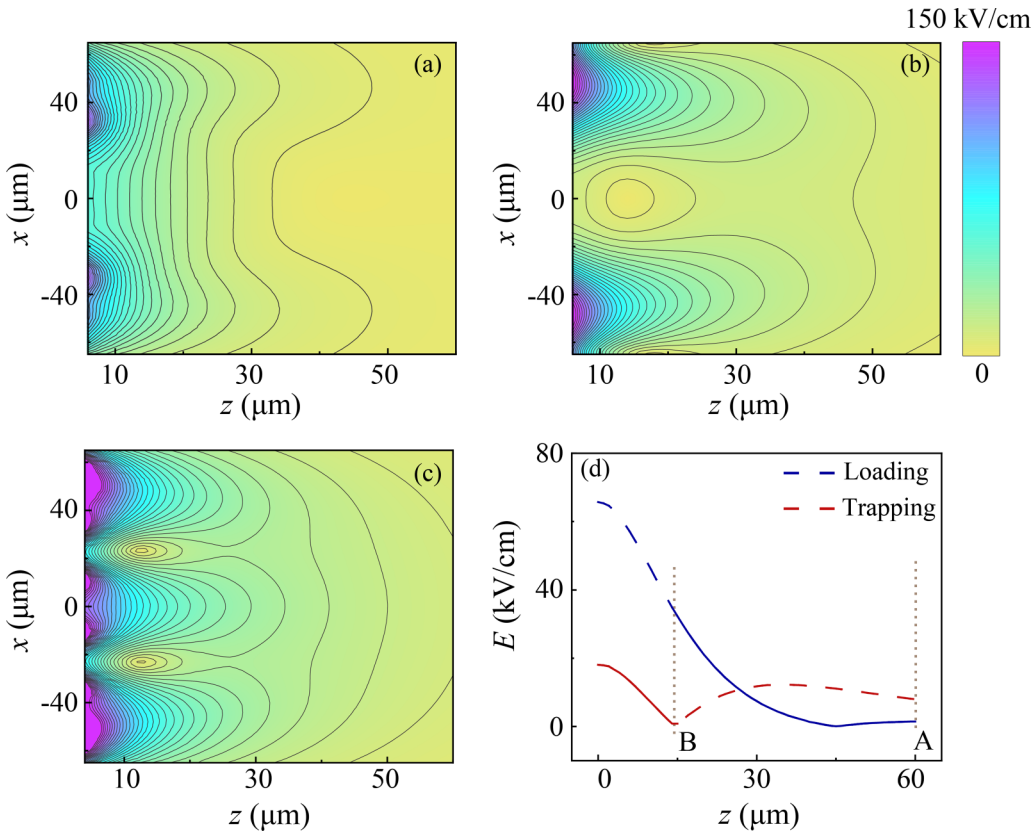

FIG. 4. The electric field distributions of loading (a), single trapping (b), and double trapping (c) in the x-z plane through the center(s) of the potential well(s). (d) Loading and trapping electric field strength in the z axis. In the color bar, violet indicates higher strength while yellowish green indicates lower strength.

A. Effectively loading beams into microtrap on a chip

In order to enhance loading efficiency, a specialized loading electric field configuration was designed that not only enables stopping molecular beams with higher kinetic energy, but also facilitates phase-space matching between the beam and the trap. Figures 4(a)–4(c) depict the distribution of the loading and the trapping electric fields in the $x-z$ plane through the minima of the potential wells. The strength of the loading electric field along the z axis is shown by the blue line in Fig. 4(d). When a packet of slowly moving cold molecules approaches the chip surface, traversing from point A to point B, the loading electric field is consistently active and precisely sufficient to bring the molecular packet to a standstill at point B. This necessitates the precise determination of applied voltage values beforehand. In Figs. 4(a) and 4(d), the set voltages are as follows: $U_1 = 90$ V, $U_2 = -150$ V, and $U_3 = U_4 = U_5 = 150$ V, which enable the deceleration of a $^{15}ND_3$ molecular beam traveling at ∼5 m/s to a standstill at point B. Upon reaching point B, the loading electric field is promptly switched to either a single-well or a double-well electric field configuration, as shown in Figs. 4(b) and 4(c), respectively. Based on this description, we performed a trajectory simulation for the ND_3 molecule. The electric fields near the chip and the force experienced by each molecule at any given location were calculated using Eqs. (1)–(4). The initial molecular beam's position and velocity distributions are Gaussian in all directions, with a six-dimensional (6D) emittance of [60 μm × 3 m/s] × [60 μm × 3 m/s] × [10 μm × 3 m/s] (in the x, y, and z axis, respectively). The beam contains 1 000 000 molecules with the initial distribution centered at $x = 0$ μm, $\upsilon_x = 0$ m/s, $y = 0$ μm, $\upsilon_y = 0$ m/s, $z = 1$ mm, and $\upsilon_z = 10$–30 m/s . The simulation starts at the exit of the hexapole downstream from the Stark decelerator, approximately 1 mm from the chip surface. Point B lies roughly 14 μm above the chip surface. For the single-well electric field configuration, the electrode voltages are set as follows: $U_1 = 200$ V, $U_2 = -200$ V, and $U_3 = U_4 = U_5 = 60$ V. For the double well, the voltages remain consistent with those of the single well, except for U_4, which is adjusted to −200V.

Figure 5 illustrates the distribution of the ND_3 molecular sample in phase space, which has been confined within the trap(s) for approximately 1 ms. Figures 5(a)–5(c) and 5(d)–5(f) correspond to single and double traps, respectively. The separatrices (depicted in red lines) represent the phase-space acceptance of the trap(s) in various directions. The molecule number density is depicted using different colors, with red and blue indicating higher and lower densities, respectively. It is evident that the molecular beam emittance matches well with the acceptance of the trap(s) in any direction.

The loading efficiency is strongly dependent on the velocity of the incident molecular beam. We have quantitatively investigated the relationship between the loading efficiency and velocity for two different electric field configurations,

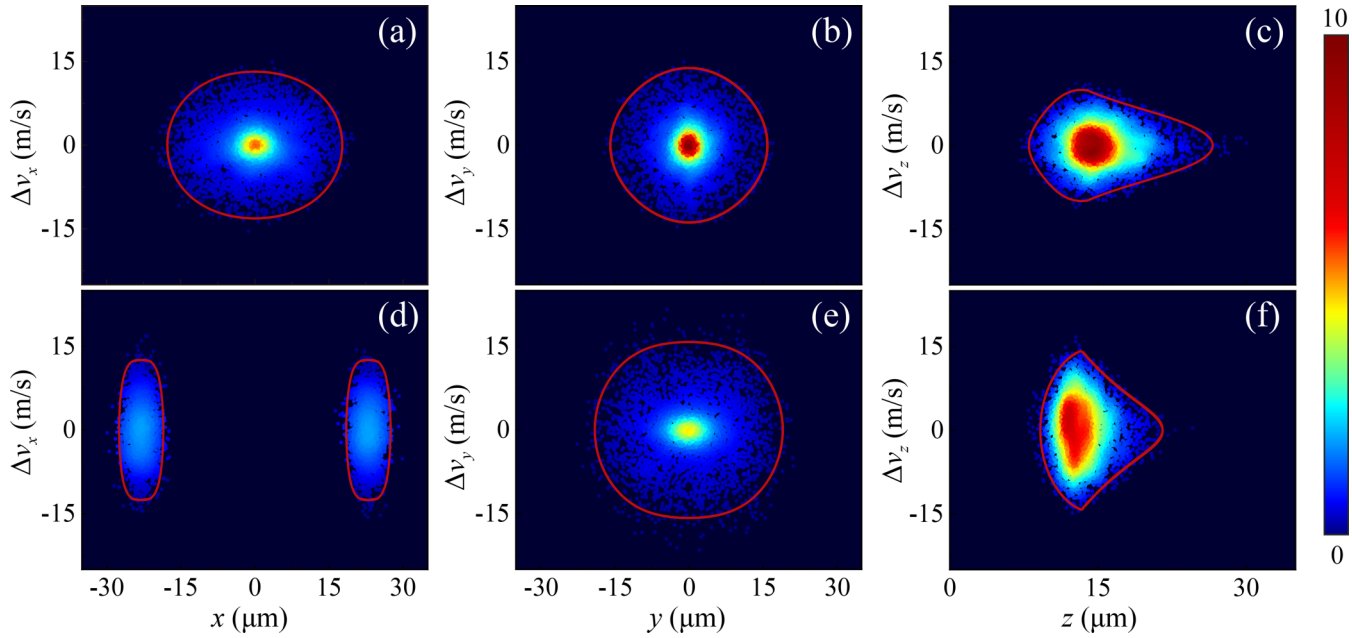

FIG. 5. Calculated phase-space distributions of ND_3 molecules confined in a single well (a)–(c) and in a double well (d)–(f) near the surface of the chip.

i.e., single trap and double traps. The results are presented in Fig. 6, where the loading efficiency η is defined as the ratio of the number of the confined packet(s) to the number of molecules in the incident beam. It is found that the maximum loading efficiency of the single trap is 0.58% when the central velocity of the molecular beam is 24 m/s. In the case of the double trap, the maximum loading efficiency reaches 0.42% when the central velocity of the molecular beam is 26 m/s. Figure 6(b) shows the number density of molecules confined in either single or double traps as a function of trapping time, indicating stable confinement of ND_3 molecules. The temperature of the confined cold molecular packets is 41.1 and 83.6 mK in single and double traps, respectively. The temperature T is defined by $(3/2)k_BT = (1/2)k_BT_L + k_BT_T$ [55], where T_L and T_T are the corresponding longitudinal and transverse temperatures of the molecular packets and are given by $T_{x,y,z} = m\Delta v_{x,y,z}^2/8\ln 2k_B$ [56] with m being the mass, $\Delta v_{x,y,z}$ the velocity spread (full width at half maximum), and k_B the Boltzmann constant.

B. Transformation between single and double well

In many application scenarios, such as confined molecule interferometry and two-qubit gate operation, the ability to bring molecules very close together and subsequently separate them is required. To verify the ability of our scheme to dynamically control double-well potentials, we utilize the method of trajectory calculation to prove this. The applied voltages for the electrodes are the same as described in the above section. A $^{15}ND_3$ molecule is used and the position and velocity distributions of the initial molecular beam are Gaussian in all directions with the six-dimensional (6D) emittance

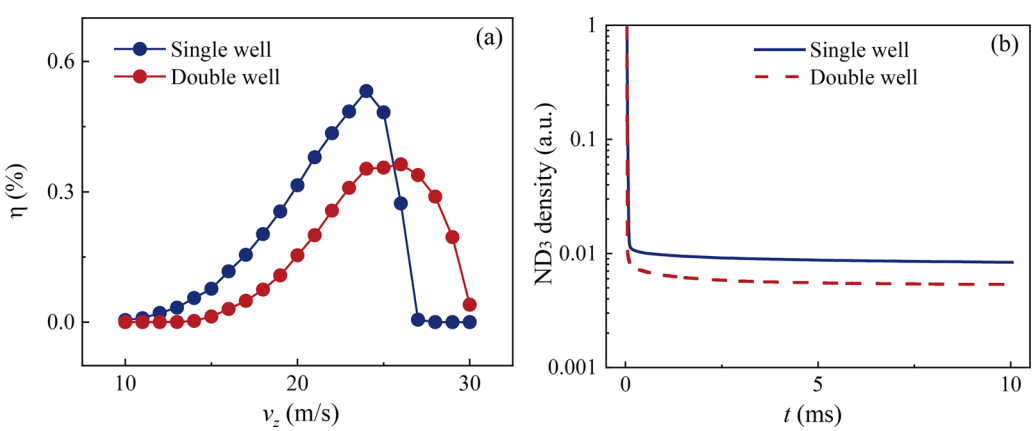

FIG. 6. (a) Calculated results for the loading efficiency of a single (blue) and a double well (red) as a function of the velocity of the incident molecular beam. (b) Calculated results of the time dependence of molecular number density for a single (blue solid line) and a double well (red dashed line).

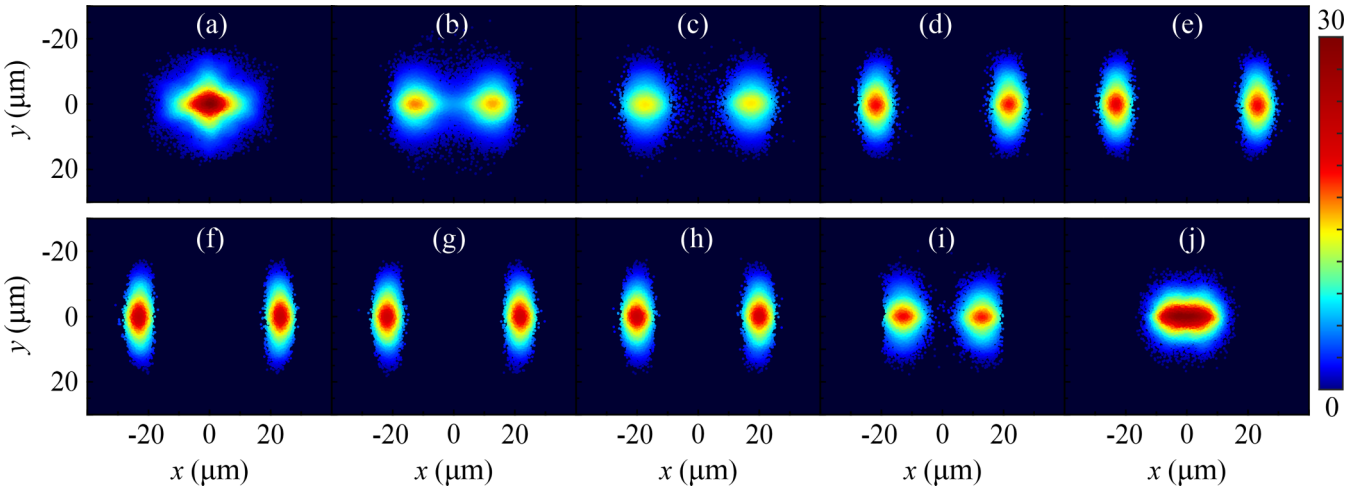

FIG. 7. Calculated results of the evolution of molecular number density from a single well to a double well (a)–(e), together with the reverse process (f)–(j).

[60 μm × 3 m/s] × [60 μm × 3 m/s] × [10 μm × 3 m/s] (in the x, y, and z axis, respectively). The beam contains 100 000 molecules with an initial distribution centered at $x = 0$ μm, $\upsilon_x = 0$ m/s, $y = 0$ μm, $\upsilon_y = 0$ m/s, $z = 14$ μm, and $\upsilon_z = 0$ m/s. The molecular packet is first confined in the single trap for 1 ms, followed by a soft transformation into a double trap within 50 μs. As can be seen in Figs. 7(a)–7(e), it is clear that the molecular packet is gradually split into two separated packets with a 45 μm distance apart, resulting in a 26% loss of molecules during the splitting process. The primary cause of molecular loss during the splitting process is the emergence of a central barrier. As the cloud of molecules is gradually split into two packets by the emerging central barrier, some molecules initially populated at the center of the single well are expelled from the trap in the z direction and subsequently lost. After holding molecules in the two traps for 1 ms, we take another 50 μs to reverse the process by merging the two wells into one well. As can be seen in Figs. 7(f)–7(j), the two separated packets gradually move together and eventually merge into one, preserving all the molecules without any loss. In comparison to the original single well, the volume of one of the double wells is significantly diminished. Alongside this reduction, the potential depth is doubled, resulting in an increased number density of molecular samples within one of the double wells during both the splitting process and the subsequent evolution stages, as illustrated in Figs. 7(b)–7(f). The above splitting and merging processes are also carried out for the HgF molecule and show similar results, which are not presented here.

The particle-based simulation described above does not account for coherence effects, as Stark-decelerated cold samples are relatively "thermal" (short de Broglie wavelength) and thus not ideally suited for molecular interferometry. Nonetheless, these simulations suffice to accurately validate the scheme's capability for preparing and manipulating cold molecules on a chip surface. Ultracold molecular samples or even molecular Bose-Einstein condensates are optimal candidates for implementing molecular interferometry. A critical aspect of an interferometer is the quantum dynamics during the splitting and recombining process. The adiabatic evolution of quantum states in a varying potential is essential to maintain coherence [6]. In other words, the ramping time should be sufficiently long for molecules to follow the potential change. It is important to note that the central barrier in this study is linearly increased. However, there are optimization methods [57] that facilitate the acceleration of both splitting and merging processes while preserving sample coherence.

The asymmetry double well is of significant interest due to its ability to produce fractional molecule distribution between the left and right wells. This feature renders numerous benefits for a series of researches with neutral molecules. For example, using an asymmetry double-well potential enables the creation of higher precision sensors for atom (or molecule) interferometry [58]. Additionally, the asymmetry double well offers opportunities for advanced Hamiltonian design, such as extended Bose-Hubbard models [59]. Figure 8(c) illustrates the characteristics of the asymmetry double well. The voltage (U_3) dependence of the barrier height (β) and the trap asymmetry Δ are shown in Figs. 8(a) and 8(b), respectively. By decreasing the voltage of U_3 (or U_5), the asymmetry of the double well can be altered, transitioning from a symmetrical double well to a singular one. In our design, an asymmetrical double well can be readily formed by applying appropriate voltages to each electrode or by modifying a symmetrical double well. We verify the process of obtaining asymmetrical wells by reducing the depth of either the left or the right potential well from a symmetrical double well. We use ND_3 and HgF molecules as testers. The results of these calculations are presented in Fig. 9, where the top row displays the configurations of the asymmetrical double well, and the corresponding molecule populations are depicted in the middle ($^{15}ND_3$) and bottom (HgF) rows. Initially, the number of $^{15}ND_3$ (or HgF) molecules in both traps is identical, as shown in Fig. 9(a). However, as the asymmetry Δ increases (with the left trap being optionally selected), the population in the left trap diminishes and eventually disappears completely. Note that there exist subtle distinctions between the evolution of the two molecular species from a symmetric double well to an asymmetric configuration, as illustrated in Fig. 9. This phenomenon can be attributed to the different forces expe-

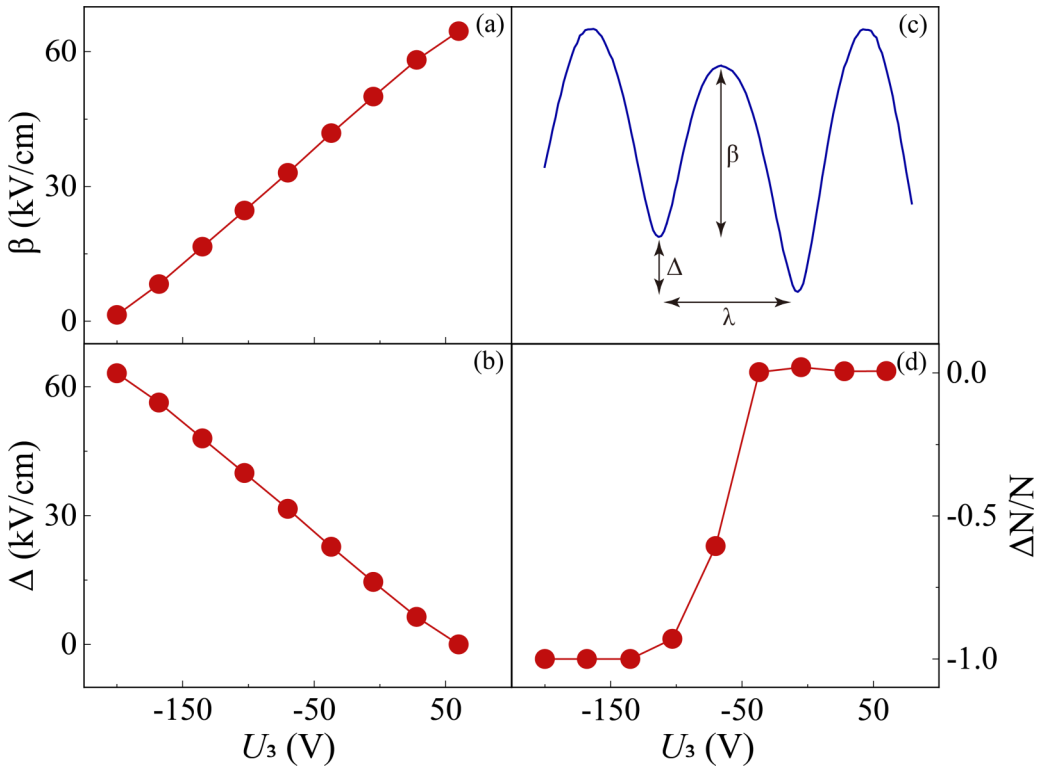

FIG. 8. Characterization of the double well as a function of the applied voltages. Barrier height β (a) and the trap asymmetry Δ (b) changes almost linearly with the voltage of U_3. (c) Illustration of the well separation λ, barrier height β, and the trap asymmetry Δ. (d) The double-well potential asymmetry dependence of the fractional number difference $\Delta N/N$. ΔN and N mean the difference in the number of molecules between two wells and the total number of molecules in both traps, respectively.

rienced by the two molecular species. $^{15}ND_3$ has a larger ratio of effective electric diploe moment to mass compared to HgF. Consequently, a greater number of $^{15}ND_3$ molecules can be captured by the trap given the same initial phase-space distribution. This effect becomes more pronounced when the trap depth is very low. As a result, the intensity distributions in

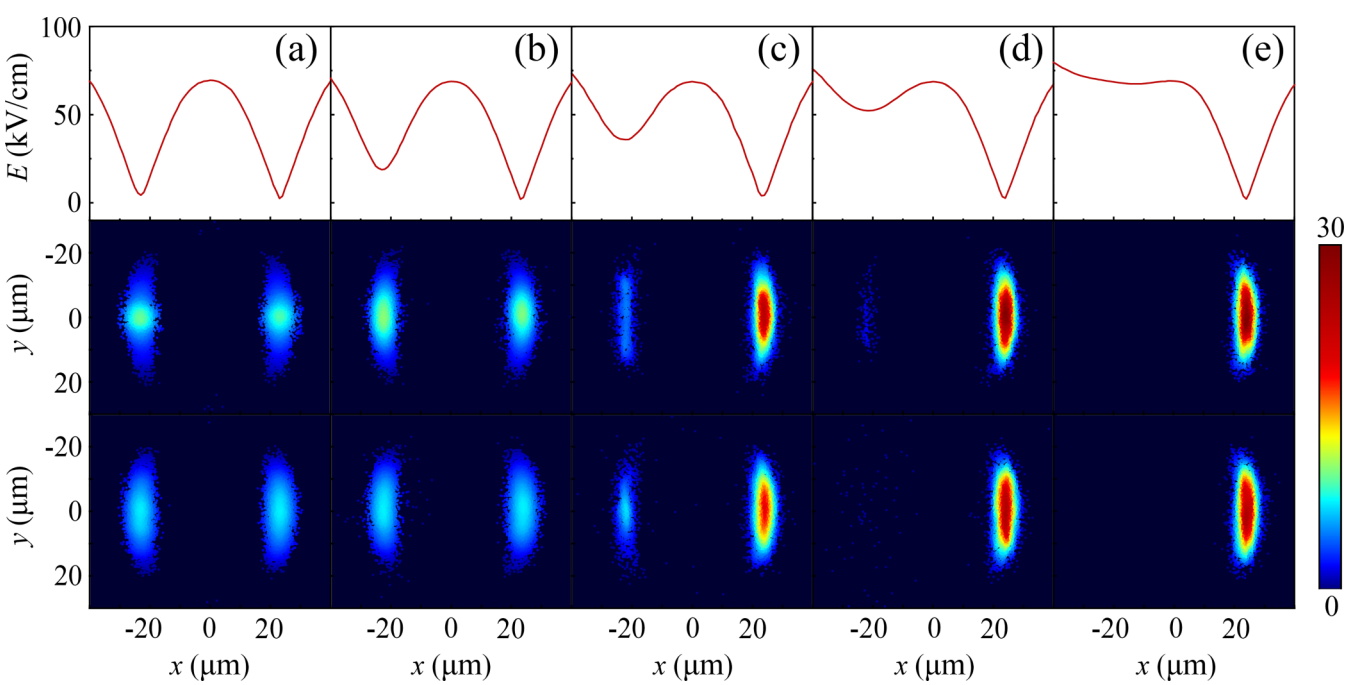

FIG. 9. Deforming a symmetry double well to an asymmetrical one (a)–(e), together with the calculated molecular population of $^{15}ND_3$ (middle row) and HgF (bottom row) in the wells.

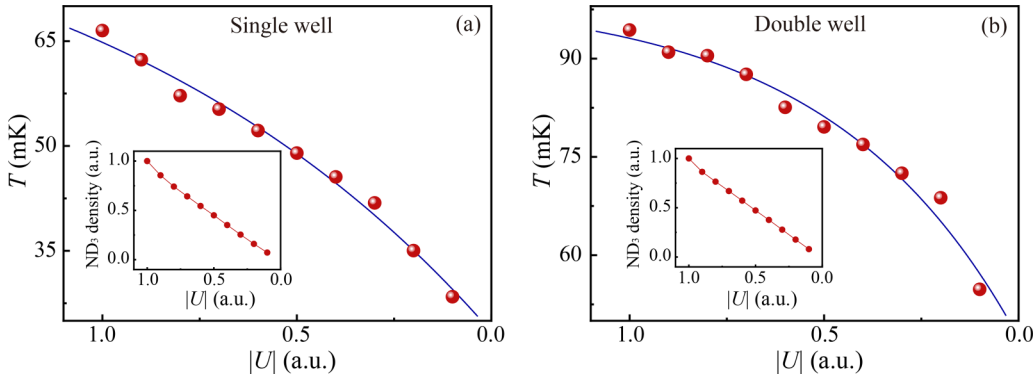

FIG. 10. The temperature of molecular samples as a function of $|U|$ for a single (a) and a double well (b), respectively. The insets depict the calculated results of $^{15}ND_3$ density versus the voltage magnitude $|U|$.

the left trap for $^{15}ND_3$ are more concentrated towards the trap center compared to HgF. As the barrier height β reaches zero, the symmetrical double well transforms into a single entity, and the fractional number difference $\Delta N/N$ also varies from 0 to -1, as depicted in Fig. 8(d).

C. Adiabatic cooling in single and double wells

Recently evaporative cooling of molecules to quantum degeneracy has been demonstrated [34]. It may be feasible to utilize the chip for preparing ultracold molecular samples and even molecular Bose-Einstein condensates using adiabatic cooling, Sisyphus cooling, or evaporative cooling methods. These methods have been previously exploited for atoms [60,61] and molecules [41] in a single chip-based trap. In our proposed scheme, the controllability of the trap depth of the microtrap on a chip facilitates adiabatic cooling of the confined molecules and achieving colder samples. We will provide examples of adiabatic cooling of trapped molecules in single trap and double traps on the chip using Monte Carlo simulation. The initial beam contains 100 000 $^{15}ND_3$ molecules with an initial distribution centered at $z = 14$ μm, $v_z = 0$m/s, $y = 0$ μm, $v_y = 0$m/s, and $x = 0$ μm, $v_x = 0$ m/s. The position and velocity distributions of the initial molecular beam are Gaussian in all directions with a 6D emittance of $[10\,\mu\text{m} \times 20\,\text{m/s}] \times [60\,\mu\text{m} \times 20\,\text{m/s}] \times [60\,\mu\text{m} \times 20\,\text{m/s}]$ (in the z, x, and y directions, respectively), which are larger than the acceptance of the chip. During the adiabatic cooling process in a single trap, the voltages applied to the chip are gradually decreased from their initial values of $U_1 = 200$ V, $U_2 = -200$ V, and $U_3 = U_4 = U_5 = 60$ V to lower values of $U_1 = 20$ V, $U_2 = -20$ V, and $U_3 = U_4 = U_5 = 6$ V over a duration of 500 μs. These reduced voltages are then maintained for an additional 500 μs. Subsequently, the voltages are slowly increased back to their original values over 500 μs and held for 300 μs. As the electrode voltage decreases, as shown in Fig. 10, the trap depth becomes shallower, allowing the hottest molecules to escape from potential wells. When the initial voltage of the single trap is reduced to 10% of the original, the temperature of the molecular sample decreases from 66.5 to 28.4 mK, as shown in Fig. 10(a). At the same time, the number of molecules decreases to 7.2% of the original, as shown in the inset of Fig. 10(a). Similarly, the adiabatic cooling process in the double trap on the chip surface operates in the same manner, with voltages changing from $U_1 = 200$ V, $U_2 = -200$ V, $U_3 = U_5 = 60$ V, and $U_4 = -200$ V to $U_1 = 20$ V, $U_2 = -20$ V, $U_3 = U_5 = 6$ V, and $U_4 = -20$ V, following the same time sequence described above. When the initial voltage of the double trap is reduced to 10% of the original, the temperature of the molecular sample decreases from 94.4 to 54.8 mK, as shown in Fig. 10(b). Simultaneously, the number of molecules decreases to 8.0% of the original, as shown in the inset of Fig. 10(b). It is worth noting that during the adiabatic cooling process, the ramping time is sufficiently long for molecules to follow the change in potential, meaning that $dT/dt \ll 1$, where dT and dt represent the trapping period and ramping time, respectively.

V. CONCLUSIONS

In conclusion, we proposed a controllable chip-based electrostatic double-well scheme characterized by its robustness, scalability, and versatility. By controlling the applied voltages on the electrodes, various operations on the double well can be conveniently achieved, such as dynamically deforming the double-well potential into a single well and vice versa, transitioning from a symmetric configuration to an asymmetric one, as well as implementing adiabatic cooling in either a single or a double well. The feasibility of this scheme is confirmed through methods involving theoretical analysis and trajectory calculations for both light ($^{15}ND_3$) and heavy ($^{202}Hg^{19}F$) molecules.

The ability to isolate molecules in our controllable double-well potentials is essential for testing a broad range of molecule-based research, ranging from quantum sensors for applications such as inertial and gravitational field sensing [11,62] to quantum tunneling effects [63], quantum entanglement [64,65], and collisions [66]. The design of the double well, which is based on a chip and scalable, also has applications in diverse fields including molecule-surface interactions [67,68] and extensions of the Bose-Hubbard model [59]. It is interesting to combine optical tweezers [69,70] with the chip-based double well, which facilitate loading and manipulation of cold molecules. The microscopic integrated double well may be utilized for applications in space-borne laboratories [71], and for exploring new frontiers in chip-based molecule science [12,72,73].

ACKNOWLEDGMENTS

This work is supported by the National Natural Science Foundation of China (Grants No. 91536218, No. 11874151, and No. 11834003), the Fundamental Research Funds for the Central Universities, the Program for Prof. of Special Appointment (Eastern Scholar) at Shanghai Institutions of Higher Learning, and the Xinjiang Tianchi Talent Program (2023).

[1] G. Möllenstedt and H. Düker, Beobachtungen und messungen an biprisma-interferenzen mit elektronenwellen, Z. Phys. **145**, 377 (1956).

[2] C. Jönsson, Elektroneninterferenzen an mehreren künstlich hergestellten Feinspalten, Z. Phys. **161**, 454 (1961).

[3] H. Rauch, W. Treimer, and U. Bonse, Test of a single crystal neutron interferometer, Phys. Lett. A **47**, 369 (1974).

[4] C. S. Adams, O. Carnal, and J. Mlynek, Atom Interferometry, in *Advances in Atomic, Molecular, and Optical Physics*, edited by B. Bederson and H. Walther (Academic, New York, 1994), Vol. 34 , pp. 1–33.

[5] M. S. Chapman, C. R. Ekstrom, T. D. Hammond, R. A. Rubenstein, J. Schmiedmayer, S. Wehinger, and D. E. Pritchard, Optics and interferometry with Na_2 molecules, Phys. Rev. Lett. **74**, 4783 (1995).

[6] A. D. Cronin, J. Schmiedmayer, and D. E. Pritchard, Optics and interferometry with atoms and molecules, Rev. Mod. Phys. **81**, 1051 (2009).

[7] R. Geiger, A. Landragin, S. Merlet, and F. Pereira Dos Santos, High-accuracy inertial measurements with cold-atom sensors, AVS Quantum Science **2**, 024702 (2020).

[8] K. Bongs, M. Holynski, J. Vovrosh, P. Bouyer, G. Condon, E. Rasel, C. Schubert, W. P. Schleich, and A. Roura, Taking atom interferometric quantum sensors from the laboratory to real-world applications, Nat. Rev. Phys. **1**, 731 (2019).

[9] D. DeMille, Diatomic molecules, a window onto fundamental physics, Phys. Today **68**(12), 34 (2015).

[10] N. R. Hutzler, Polyatomic molecules as quantum sensors for fundamental physics, Quantum Sci. Technol. **5**, 044011 (2020).

[11] D. DeMille, N. R. Hutzler, A. M. Rey, and T. Zelevinsky, Quantum sensing and metrology for fundamental physics with molecules, Nat. Phys. **20**, 741 (2024).

[12] M. S. Safronova, D. Budker, D. DeMille, D. F. Jackson Kimball, A. Derevianko, and C. W. Clark, Search for new physics with atoms and molecules, Rev. Mod. Phys. **90**, 025008 (2018).

[13] J. J. Hudson, D. M. Kara, I. J. Smallman, B. E. Sauer, M. R. Tarbutt, and E. A. Hinds, Improved measurement of the shape of the electron, Nature (London) **473**, 493 (2011).

[14] V. Andreev, D. G. Ang, D. DeMille, J. M. Doyle, G. Gabrielse, J. Haefner, N. R. Hutzler, Z. Lasner, C. Meisenhelder, B. R. O'Leary, C. D. Panda, A. D. West, E. P. West, and X. Wu (ACME Collaboration), Improved limit on the electric dipole moment of the electron, Nature (London) **562**, 355 (2018).

[15] C. Chin, V. V. Flambaum, and M. G. Kozlov, Ultracold molecules: New probes on the variation of fundamental constants, New J. Phys. **11**, 055048 (2009).

[16] E. J. Salumbides, J. C. J. Koelemeij, J. Komasa, K. Pachucki, K. S. E. Eikema, and W. Ubachs, Bounds on fifth forces from precision measurements on molecules, Phys. Rev. D **87**, 112008 (2013).

[17] M. Borkowski, A. A. Buchachenko, R. Ciuryło, P. S. Julienne, H. Yamada, Y. Kikuchi, Y. Takasu, and Y. Takahashi, Weakly bound molecules as sensors of new gravitylike forces, Sci. Rep. **9**, 14807 (2019).

[18] P. W. Graham and S. Rajendran, Axion dark matter detection with cold molecules, Phys. Rev. D **84**, 055013 (2011).

[19] R. Folman, P. Krüger, J. Schmiedmayer, J. Denschlag, and C. Henkel, *Microscopic Atom Optics: From Wires to an Atom Chip* (Academic Press, New York, 2002), Vol. 48.

[20] D. Li, W. He, S. Shi, B. Wu, Y. Xiao, Q. Lin, and L. Li, Review of atom chips for absolute gravity sensors, Sensors **23**, 5089 (2023).

[21] J. Reichel and V. Vuletic, *Atom Chips* (Wiley, New York, 2011).

[22] T. P. Softley, Cold and ultracold molecules in the twenties, Proc. R. Soc. A **479**, 20220806 (2023).

[23] T. Langen, G. Valtolina, D. Wang, and J. Ye, Quantum state manipulation and cooling of ultracold molecules, Nat. Phys. **20**, 702 (2024).

[24] H. L. Bethlem, G. Berden, and G. Meijer, Decelerating neutral dipolar molecules, Phys. Rev. Lett. **83**, 1558 (1999).

[25] E. Narevicius, C. G. Parthey, A. Libson, M. F. Riedel, U. Even, and M. G. Raizen, Towards magnetic slowing of atoms and molecules, New J. Phys. **9**, 96 (2007).

[26] E. Vliegen, H. J. Wörner, T. P. Softley, and F. Merkt, Nonhydrogenic effects in the deceleration of Rydberg atoms in inhomogeneous electric fields, Phys. Rev. Lett. **92**, 033005 (2004).

[27] Y. Ji, Q. Liu, Y. Liu, T. Yang, S. Hou, and J. Yin, Design of a ring-shaped traveling-wave Zeeman decelerator for both light and heavy molecules, Phys. Rev. A **108**, 043115 (2023).

[28] H. Guo, Y. Ji, Q. Liu, T. Yang, S. Hou, and J. Yin, Controllable three-dimensional electrostatic lattices for manipulation of cold polar molecules, Phys. Rev. A **105**, 053108 (2022).

[29] E. S. Shuman, J. F. Barry, and D. DeMille, Laser cooling of a diatomic molecule, Nature (London) **467**, 820 (2010).

[30] J. F. Barry, D. J. McCarron, E. B. Norrgard, M. H. Steinecker, and D. DeMille, Magneto-optical trapping of a diatomic molecule, Nature (London) **512**, 286 (2014).

[31] S. Truppe, H. J. Williams, M. Hambach, L. Caldwell, N. J. Fitch, E. A. Hinds, B. E. Sauer, and M. R. Tarbutt, Molecules cooled below the Doppler limit, Nat. Phys. **13**, 1173 (2017).

[32] N. B. Vilas, C. Hallas, L. Anderegg, P. Robichaud, A. Winnicki, D. Mitra, and J. M. Doyle, Magneto-optical trapping and sub-Doppler cooling of a polyatomic molecule, Nature (London) **606**, 70 (2022).

[33] L. De Marco, G. Valtolina, K. Matsuda, W. G. Tobias, J. P. Covey, and J. Ye, A degenerate Fermi gas of polar molecules, Science **363**, 853 (2019).

[34] A. Schindewolf, R. Bause, X.-Y. Chen, M. Duda, T. Karman, I. Bloch, and X.-Y. Luo, Evaporation of microwave-shielded polar

molecules to quantum degeneracy, Nature (London) **607**, 677 (2022).

[35] G. Valtolina, K. Matsuda, W. G. Tobias, J.-R. Li, L. De Marco, and J. Ye, Dipolar evaporation of reactive molecules to below the Fermi temperature, Nature (London) **588**, 239 (2020).

[36] N. Bigagli, W. Yuan, S. Zhang, B. Bulatovic, T. Karman, I. Stevenson, and S. Will, Observation of Bose–Einstein condensation of dipolar molecules, Nature (London) **631**, 289 (2024).

[37] S. A. Meek, H. Conrad, and G. Meijer, Trapping molecules on a chip, Science **324**, 1699 (2009).

[38] S. A. Meek, G. Santambrogio, B. G. Sartakov, H. Conrad, and G. Meijer, Suppression of nonadiabatic losses of molecules from chip-based microtraps, Phys. Rev. A **83**, 033413 (2011).

[39] A. Deller, M. H. Rayment, and S. D. Hogan, Slow decay processes of electrostatically trapped Rydberg NO molecules, Phys. Rev. Lett. **125**, 073201 (2020).

[40] S. Marx, D. Adu Smith, G. Insero, S. A. Meek, B. G. Sartakov, G. Meijer, and G. Santambrogio, Measuring and manipulating the temperature of cold molecules trapped on a chip, Phys. Rev. A **92**, 063408 (2015).

[41] M. Zeppenfeld, B. G. U. Englert, R. Glöckner, A. Prehn, M. Mielenz, C. Sommer, L. D. Van Buuren, M. Motsch, and G. Rempe, Sisyphus cooling of electrically trapped polyatomic molecules, Nature (London) **491**, 570 (2012).

[42] B. G. U. Englert, M. Mielenz, C. Sommer, J. Bayerl, M. Motsch, P. W. H. Pinkse, G. Rempe, and M. Zeppenfeld, Storage and adiabatic cooling of polar molecules in a microstructured trap, Phys. Rev. Lett. **107**, 263003 (2011).

[43] S. Y. Hou, B. Wei, L. Z. Deng, and J. P. Yin, Chip-based microtrap arrays for cold polar molecules, Phys. Rev. A **96**, 063416 (2017).

[44] X. Y. Xu, T. Yang, S. Y. Hou, and J. P. Yin, Controllable chip-based beam splitter for cold polar molecules, Phys. Rev. A **100**, 013411 (2019).

[45] J. P. McGilligan, K. Gallacher, P. F. Griffin, D. J. Paul, A. S. Arnold, and E. Riis, Micro-fabricated components for cold atom sensors, Rev. Sci. Instrum. **93**, 091101 (2022).

[46] T. Schumm, S. Hofferberth, L. M. Andersson, S. Wildermuth, S. Groth, I. Bar-Joseph, J. Schmiedmayer, and P. Krüger, Matter-wave interferometry in a double well on an atom chip, Nat. Phys. **1**, 57 (2005).

[47] Y. Shin, C. Sanner, G.-B. Jo, T. A. Pasquini, M. Saba, W. Ketterle, D. E. Pritchard, M. Vengalattore, and M. Prentiss, Interference of Bose-Einstein condensates split with an atom chip, Phys. Rev. A **72**, 021604(R) (2005).

[48] G.-B. Jo, J.-H. Choi, C. A. Christensen, T. A. Pasquini, Y.-R. Lee, W. Ketterle, and D. E. Pritchard, Phase-sensitive recombination of two Bose-Einstein condensates on an atom chip, Phys. Rev. Lett. **98**, 180401 (2007).

[49] G.-B. Jo, Y. Shin, S. Will, T. A. Pasquini, M. Saba, W. Ketterle, D. E. Pritchard, M. Vengalattore, and M. Prentiss, Long phase coherence time and number squeezing of two Bose-Einstein condensates on an atom chip, Phys. Rev. Lett. **98**, 030407 (2007).

[50] J. Alexander, V. Prieto, C. Rowlett, W. Golding, and P. Lee, Manipulations of cold atoms on a chip: Double well potential and 1D Bose gas, Proc. SPIE **8400**, 840004 (2012).

[51] F. Borselli, M. Maiwöger, T. Zhang, P. Haslinger, V. Mukherjee, A. Negretti, S. Montangero, T. Calarco, I. Mazets, M. Bonneau *et al.*, Two-particle interference with double twin-atom beams, Phys. Rev. Lett. **126**, 083603 (2021).

[52] Z. Yang, J. Li, Q. Lin, L. Xu, H. Wang, T. Yang, and J. Yin, Laser-cooled HgF as a promising candidate to measure the electric dipole moment of the electron, Phys. Rev. A **99**, 032502 (2019).

[53] S. A. Meek, H. Conrad, and G. Meijer, A Stark decelerator on a chip, New J. Phys. **11**, 055024 (2009).

[54] J. Van Veldhoven, H. L. Bethlem, M. Schnell, and G. Meijer, Versatile electrostatic trap, Phys. Rev. A **73**, 063408 (2006).

[55] G. Scoles, *Atomic and Molecular Beam Methods* (Oxford University Press, New York, 1988).

[56] M. Gupta and D. Herschbach, A mechanical means to produce intense beams of slow molecules, J. Phys. Chem. A **103**, 10670 (1999).

[57] W. Hänsel, J. Reichel, P. Hommelhoff, and T. Hänsch, Trapped-atom interferometer in a magnetic microtrap, Phys. Rev. A **64**, 063607 (2001).

[58] B. V. Hall, S. Whitlock, R. Anderson, P. Hannaford, and A. I. Sidorov, Condensate splitting in an asymmetric double well for atom chip based sensors, Phys. Rev. Lett. **98**, 030402 (2007).

[59] M. A. Baranov, M. Dalmonte, G. Pupillo, and P. Zoller, Condensed matter theory of dipolar quantum gases, Chem. Rev. **112**, 5012 (2012).

[60] A. Kastberg, W. D. Phillips, S. L. Rolston, R. J. C. Spreeuw, and P. S. Jessen, Adiabatic cooling of cesium to 700 nK in an optical lattice, Phys. Rev. Lett. **74**, 1542 (1995).

[61] J. Märkle, A. J. Allen, P. Federsel, B. Jetter, A. Günther, J. Fortágh, N. P. Proukakis, and T. E. Judd, Evaporative cooling of cold atoms at surfaces, Phys. Rev. A **90**, 023614 (2014).

[62] J. Ye and P. Zoller, Essay: Quantum sensing with atomic, molecular, and optical platforms for fundamental physics, Phys. Rev. Lett. **132**, 190001 (2024).

[63] M. Albiez, R. Gati, J. Fölling, S. Hunsmann, M. Cristiani, and M. K. Oberthaler, Direct observation of tunneling and nonlinear self-trapping in a single bosonic Josephson junction, Phys. Rev. Lett. **95**, 010402 (2005).

[64] M. F. Riedel, P. Böhi, Y. Li, T. W. Hänsch, A. Sinatra, and P. Treutlein, Atom-chip-based generation of entanglement for quantum metrology, Nature (London) **464**, 1170 (2010).

[65] L. Fu and J. Liu, Quantum entanglement manifestation of transition to nonlinear self-trapping for Bose-Einstein condensates in a symmetric double well, Phys. Rev. A **74**, 063614 (2006).

[66] T. Calarco, E. A. Hinds, D. Jaksch, J. Schmiedmayer, J. I. Cirac, and P. Zoller, Quantum gates with neutral atoms: Controlling collisional interactions in time-dependent traps, Phys. Rev. A **61**, 022304 (2000).

[67] J. D. Perreault and A. D. Cronin, Observation of atom wave phase shifts induced by van der Waals atom-surface interactions, Phys. Rev. Lett. **95**, 133201 (2005).

[68] A. Laliotis, B.-S. Lu, M. Ducloy, and D. Wilkowski, Atom-surface physics: A review, AVS Quantum Sci. **3**, 043501 (2021).

[69] L. Anderegg, L. W. Cheuk, Y. Bao, S. Burchesky, W. Ketterle, K.-K. Ni, and J. M. Doyle, An optical tweezer array of ultracold molecules, Science **365**, 1156 (2019).

[70] N. B. Vilas, P. Robichaud, C. Hallas, G. K. Li, L. Anderegg, and J. M. Doyle, An optical tweezer array of ultracold polyatomic molecules, Nature (London) **628**, 282 (2024).

[71] D. Becker, M. D. Lachmann, S. T. Seidel, H. Ahlers, A. N. Dinkelaker, J. Grosse, O. Hellmig, H. Müntinga, V. Schkolnik, T. Wendrich *et al.*, Space-borne Bose–Einstein condensation for precision interferometry, Nature (London) **562**, 391 (2018).

[72] C. Wang, X. Yi, J. Mawdsley, M. Kim, Z. Wang, and R. Han, An on-chip fully electronic molecular clock based on sub-terahertz rotational spectroscopy, Nat. Electron. **1**, 421 (2018).

[73] J. Chen, K. Keiler, G. Xianlong, and P. Schmelcher, Impurity-induced quantum chaos for an ultracold bosonic ensemble in a double well, Phys. Rev. A **104**, 033315 (2021).